Structural and size evolution of indium nanoparticles embedded in aluminum synthesized by ion implantation*

Yan-Xia Yan(晏艳霞), Meng Liu(刘孟), Mei-Juan Hu(胡梅娟), Hong-Zhi Zhu(朱宏志), and Huan Wang(王欢)†

Institute of Materials, China Academy of Engineering Physics, Jiangyou 621907, *China*

(Received 31 May 2017; revised manuscript received 4 September 2017; published online 20 November 2017)

The structural and the size evolution of embedded In nanoparticles in Al synthesized by ion implantation and subsequent annealing are experimentally investigated. The average radius r of In nanoparticles is determined as a function of annealing time in a temperature range between 423 K and 453 K. The structural transition of In nanoparticles with the crystallographic orientation In (200)[002]||Al (200)[002] is observed to change into In (111)[1$\underline{1}$0]||Al (002)[110] with a critical particle radius between 2.3 nm and 2.6 nm. In addition, the growth of In nanoparticles in the annealing process is evidently governed by the diffusion limited Ostwald ripening. By further analyzing the experimental data, values of diffusion coefficient and activation energy are obtained.

Keywords: ion implantation, indium nanoparticles, size evolution

PACS: 61.05.cp, 61.46.Hk, 61.72.U– **DOI:** 10.1088/1674-1056/26/12/126101

1. Introduction

Nanoparticles are frequently characterized by novel structural,[1,2] magnetic,[3] electronic,[4] optical,[5] and superconducting[6,7] properties that are significantly different from those of either the corresponding bulk or single molecule. The differences between small particles and bulk materials are observed to be increasingly pronounced as materials are formed on an ever reducing length scale. Such differences stimulate a growing worldwide effort that cuts across many research subjects and areas which focus on the synthesis and characterization of an increasingly variety of nanophase particles. The motivation for such research activities is driven by both fundamental interest in characteristics of small particles and by their numerous possible applications.

Indium is an element with a relatively high bulk superconducting transition temperature at 4.2 K and a relatively low bulk melting point at 430 K.[8] Previous investigations show that indium nanoparticles present special thermal,[9] optical,[10] and superconducting[11] properties, which are synthesized by various techniques such as solvated metal atom dispersion,[12] ion implantation,[13] gas condensation,[14] etc.

As one of the well-established methods of fabricating individual embedded nanoparticles, high fluence implantation of an insoluble element in a crystalline matrix and subsequent annealing, resulting in the segregation of implanted specimen, formation and growth of nanoscale particles in matrix, have been used in various studies.[15–18] The control of average size of nanoparticles in the implantation or subsequent annealing process is one of the challenging issues of this technique, as the properties of nanoparticles depend strongly on their size. Thus, a precise understanding of the influences of synthesis parameters, such as implantation fluence, annealing time and temperature, on the evolution of particle size (distribution) is of paramount importance.

The purpose of this work is to investigate the formation and growth of In nanoparticles in an Al matrix in the annealing process after ion implantation. The x-ray diffraction (XRD) is employed to evaluate the average particle size as a function of annealing temperature and time. The results are compared with the existing model prediction to explain the growth kinetics of In nanoparticles in the annealing process. In addition, the estimates of the diffusion coefficient and activation energy are obtained in the annealing process. Moreover, the critical size of In nanoparticles with different crystallographic orientations with respect to the Al matrix is determined.

2. Experiment

Single-crystal Al (100) wafer was implanted with 70-keV In^+ ions. In order to reduce sample heating, the current density in the ion implantation process was maintained below 0.3 $\mu A \cdot cm^{-2}$. After ion implantation, samples were annealed in a quartz tube furnace under flowing N_2 for different time intervals varying between 0.5 hour and 9 hours at temperatures of 423 K, 438 K, and 453 K, respectively.

A collimated 2.023-MeV He^+ beam produced by a 5SDH-2 Pelletron was used for the Rutherford backscattering (RBS) measurements. The backscattered particles were detected at 168° with respect to the beam direction by using an Au–Si barrier detector with the energy resolution about 18 keV, corresponding to a depth resolution $\sim$ 1 nm.

*Project supported by the National Natural Science Foundation of China (Grant No. 11505160) and the Director Foundation of Institute of Materials, Chinese Academy of Engineering Physics (Grant No. SJZD201406).

†Corresponding author. E-mail: wanghuan_2001@163.com

© 2017 Chinese Physical Society and IOP Publishing Ltd

Conventional x-ray diffraction measurements were carried out with the Cu K_α line in a D8 Discover diffractometer. The θ–2θ scans were performed with 2θ typically ranging from 25° to 75° at 0.02° per step. The x-ray wavelength is 0.1542 nm. The crystallite size (d) of embedded In nanoparticles is calculated from Scherrer formula:

$$d = 0.9\lambda / B\cos\theta, \tag{1}$$

where λ is the wavelength of x-ray, θ the Bragg angle, and B the full width of half maximum of 2θ in radians. By assuming a spherical shape, the average radius ($r = d/2$) of the In nanoparticles can then be deduced from the XRD patterns.

3. Results and discussion

The RBS is used to determine the implanted In fluence after implantation. Figure 1 shows the random RBS spectrum of the sample with an implantation flunence of 1.0×10^{16} cm^{-2}. The detector geometry is shown in the inset.

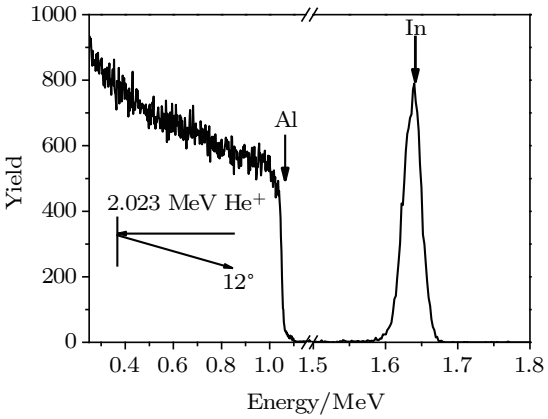


Fig. 1. Random RBS spectrum of the implanted sample with an implantation fluence of 1×10^{16} cm^{-2}. The arrows marked with In and Al indicate the energies for backscattering from In atoms and Al atoms.

The depth profile of implanted In atoms, which is deduced from RBS spectrum for the implanted samples, is shown in Fig. 2. Compared with the simulated depth profile obtained from the TRIM program,[19] the In depth profile in our implanted samples is evidently broadened. Such an observed phenomenon is expected to be mainly attributed to the migration of In atoms in Al, caused by ion irradiation heating in the implantation process.

Figure 3 shows the θ–2θ scans of virgin Al and the implanted samples for different annealing times at 438 K. The small sharp peak located at 40.1° is due to the contribution of the residual Cu K_β radiation to the Al (200) diffraction peak. In the annealed samples, the only detectable diffraction peaks at $2\theta \approx 37.7°$ are observed with annealing time smaller than 1 hour, confirming that the In nanoparticles are highly orientated with respect to the host Al matrix.[20] The In diffraction peaks sharpen with increasing annealing time, indicating that the size of In nanoparticles increases.

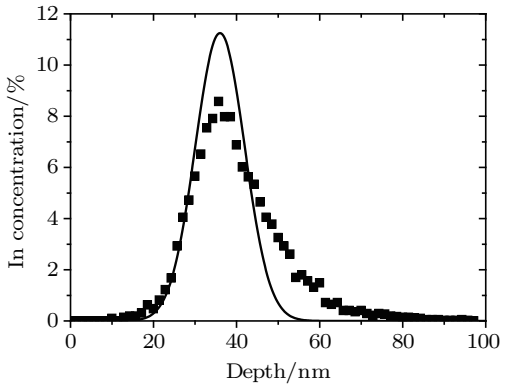


Fig. 2. In depth profile in Al (■) obtained from RBS. The solid line represents theoretical profile obtained from the TRIM program.

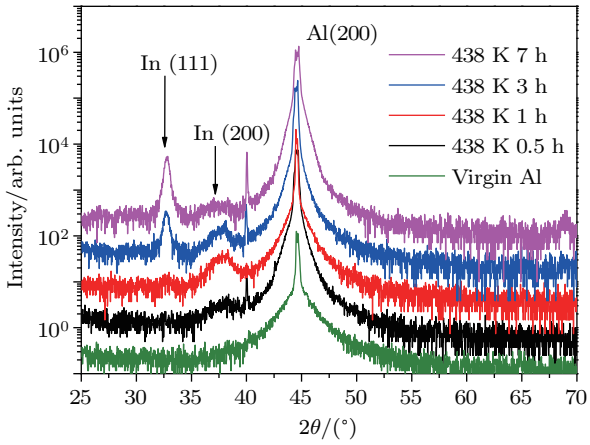


Fig. 3. (color online) XRD θ–2θ scans for virgin Al and annealed implanted samples for different annealing times. The data sets are shifted vertically for clarity.

Azimuthal Φ scans of the diffraction planes, which are not parallel to the sample surface (i.e., tilted by an angle χ with respect to the sample surface), are used to determine the lattice structure of In nanoparticles and reveal their in-plane crystallographic orientation with respect to the Al matrix. Figure 4 shows Φ scans of the sample annealed at 438 K for 1 h for the In (111) diffraction with $2\theta \approx 32.5°$ and the Al (111) diffraction with $2\theta \approx 38.5°$, respectively. The four-fold symmetry, with $\chi \approx 54.8°$, is consistent with the fcc-In (111) Φ scan. The peak positions of In (111) are coincident with the ones of Al (111), indicating an epitaxial relationship between the In nanoparticles and the Al matrix. Therefore we conclude that the fcc In nanoparticles are crystallographically oriented with respect to the Al matrix according to In (200)[002]‖Al (200)[002], consistent with previous investigations.[13,20]

By extending the annealing time, a new diffraction peak located at $2\theta \approx 32.8°$ appears with an annealing duration of 3 hours as shown in Fig. 3, which corresponds the In (111) diffraction peak. Thus, a new type of In nanoparticle in Al with crystallographic orientation In (111)‖Al (002) is evident. Taking the Al (200) peak as a reference, the lattice constant of the embedded fcc In nanoparticles is deduced to be 0.469 nm.

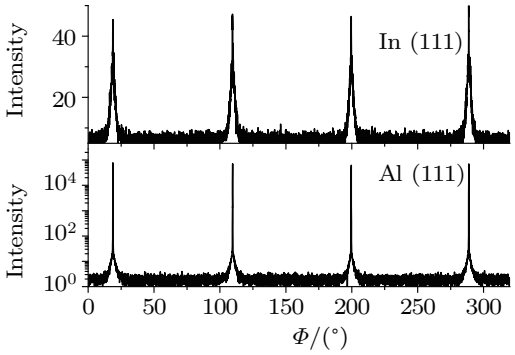


Fig. 4. XRD Φ scans of the sample for fcc-In (111) and Al (111) ($\chi \sim 54.8^\circ$).

Interestingly, previous investigations by Kemerink *et al.* showed that such an orientation transition of embedded In nanoparticles in Al–In system containing 125 at.% ppm indium is determined by annealing temperature, which equals 573 K.[21] However, in our experiments, the structural transition happens at 438 K, i.e., 135 K or less. Based on the observed results, it can be assumed that the change of crystallographic orientation for In nanoparticles in Al is size-dependent. In our implanted samples, the average indium content in implantation regions is estimated to be $\sim 5\%$ (Fig. 2). The higher intensity of In in Al indicates a faster size evolution of embedded particles by incorporating the dissolved In monomers compared with the samples with relatively low In content. In Fig. 3, it is found that such a structural orientation transition of the embedded In nanoparticles occurs at the annealing times of 1 hour and 3 hours with the annealing temperature at 438 K. Thus, the critical transition radius of In nanoparticles in Al matrix is experimentally determined from the In (200) diffraction peak, which varies between 2.3 nm and 2.6 nm. As particles reach to the critical size, their orientation with respect to the Al matrix changes from In (200)[002]||Al (200)[002] to In (111)[1$\underline{1}$0]||Al (002)[110] in order to lower the interfacial energy. Such an assumption can be proven by previous investigations on the melting point of In nanoparticles in Al, which shows that the superheating of In nanoparticles is attributed to the suppression of interface nucleation by the epitaxial interfaces between the Al matrix and the In nanoparticles.[13] In addition, with increasing particle size, the surface-to-volume ratio decreases. Thus, the role of the low-energy In/Al interfaces in achieving superheating is expected to be suppressed,[13] which is consistent with the prediction by molecular dynamics simulations.[22]

Figure 5 shows the average particle radius as a function of annealing time at different temperatures, obtained by using Eq. (1). Obviously, the average particle size increases with annealing time increasing. At 423 K, the average particle radius varies between 1.5 nm and 2.1 nm, which is smaller than the critical transition size indicating that embedded In nanoparticles present the orientation relationship with respect to the Al matrix as In (200)[002]||Al (200)[002]. As the annealing temperature reaches to 438 K and 453 K, the average particle size can be deduced from the In (111) diffraction peak.

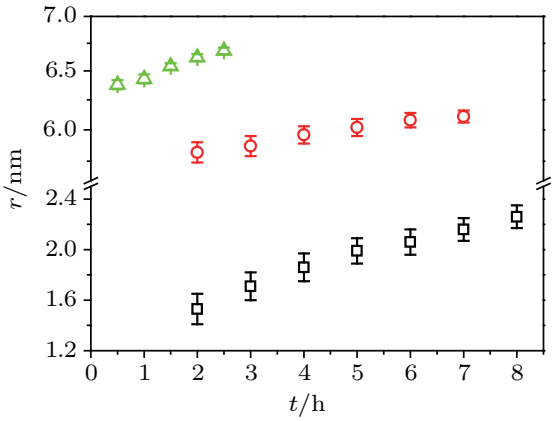


Fig. 5. (color online) Plots of average particle radius r versus annealing time t at 423 K (□), 438 K (◯), and 453 K (△).

In Fig. 3, the intensity of In (111) peak increases with the decrease of In (002) peak. It gives a strong indication that Ostwald ripening happens in the annealing process, i.e., the larger In nanoparticles grow at the expense of smaller In nanoparticles. In order to explain the size evolution of the In nanoparticles in the annealing process, the Lifshitz–Slyozov–Wagner (LSW) theory is used on the assumption that the crystallite has a spherical shape.[23,24] In the LSW theory, the growth kinetics of spherical precipitates during particles coarsening is described as

$$r^3 - r_0^3 = \frac{8\gamma c_e D\Omega^2}{9RT}t, \tag{2}$$

where r is the average particle radius; t is the annealing time; γ is the interface energy, which equals 30 mJ·m^{-2};[25] c_e is the solubility limit, which equals 0.045 at.%, i.e., 45 mol·m^{-3};[26] D is the diffusion coefficient of In in Al; Ω is the molar volume of the solute, i.e., 15.73×10^{-6} m^3·mol^{-1};[8] R equals 8.3144 J·mol^{-1}·K^{-1}; T is the absolute temperature.

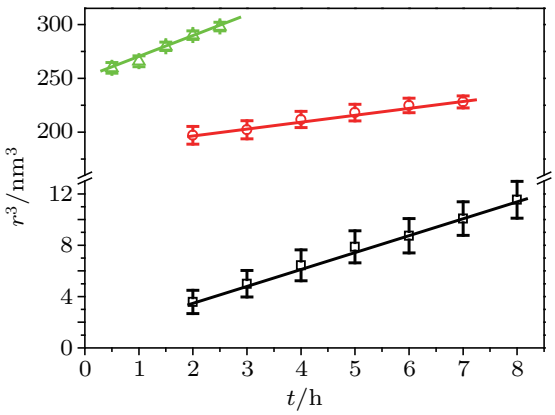


Fig. 6. (color online) Plots of r^3 versus annealing time t at 423 K (□), 438 K (◯), and 453 K (△). The solid lines refer to the linear fittings to the experimental data.

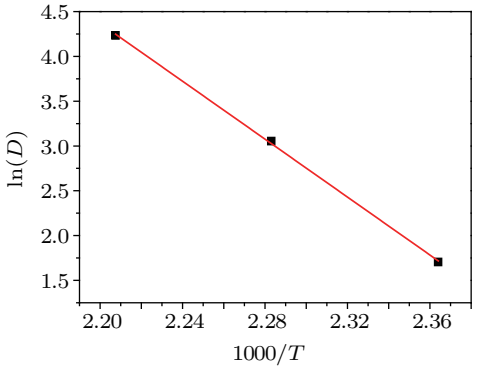


Fig. 7. (color online) Plot of $\ln(D)$ versus reciprocal annealing temperature $1000/T$. The solid line (—) represents the linear fitting to the experimental data.

To better demonstrate the growth of embedded In nanoparticles in the annealing process, we show in Fig. 6 the plots of r^3 of the growing particles versus annealing time t at 423 K, 438 K, and 453 K, respectively. There is a linear relationship between r^3 and t, indicating the Ostwald ripening of embedded In nanoparticles. According to Eq. (2), the diffusion coefficient D can be deduced to be 5.5 $nm^2 \cdot s^{-1}$, 21.2 $nm^2 \cdot s^{-1}$, and 69.0 $nm^2 \cdot s^{-1}$, respectively, at 423 K, 438 K, and 453 K. Since $D = D_0 \exp(-E_a/k_B T)$, where D_0 is a diffusivity prefactor, E_a is the diffusion activation energy, and k_B is the Boltzmann constant. In Fig. 7, we plot ln$D$ versus reciprocal annealing temperature $1000/T$. A linear fitting of the data in Fig. 7 leads to an activation energy of 1.39 eV for this diffusion-controlled Ostwald ripening process. The activation energy is similar to value found for other non-transition solutes in Al,[27–30] which varies between 1.21 eV and 1.40 eV. Since the activation energy for Al self-diffusion lies between a minimum of 1.25 eV obtained from the NMR measurements,[31] and an upper limit of 1.49 eV from tracer diffusion studies.[32] It confirms that the In-vacancy binding energy is small.

4. Conclusions

We investigate the clustering process of In atoms in a single crystalline Al matrix. Indium nanoparticles with the crystallographic orientations In (200)[002]||Al (200)[002] evidently change into In (111)[1$\underline{1}$0]||Al (002)[110] with a critical particle radius varies between 2.3 nm to 2.6 nm. By analyzing the average particle radius as a function of annealing time and annealing temperature, we observe that the growth of embedded In nanoparticles is governed by diffusion-controlled Ostwald ripening, with an activation energy of 1.39 eV. Moreover, the diffusion coefficients of In atoms in Al ranging from 5.5 $nm^2 \cdot s^{-1}$ to 69.0 $nm^2 \cdot s^{-1}$ is obtained in a temperature range between 423 K and 453 K.

References

[1] Ajibade P A and Botha N L 2017 *Nanomaterials* **7** 32
[2] Heinz H, Pramanik C, Heinz Q, Ding Y F, Mishra R K, Marchon D, Flatt F J, Estrela-Lopis I, Llop J, Moya S and Ziolo R F 2017 *Surf. Sci. Rep.* **72** 1
[3] Obaidat I M, Issa B and Haik Y 2015 *Nanomaterials* **5** 63
[4] Pandey R R, Fukumori M, Yousefi A T, Eguchi M, Tanaka D, Ogawa T and Tanaka H 2017 *Nanotechnology* **28** 175704
[5] Kosinova A, Wang D, Baradács E, Parditka B, Kups T, Klinger L, Erdélyi Z, Schaaf P and Rabkin E 2017 *Acta Materialia* **127** 108
[6] Bose S and Ayyub P 2014 *Rep. Prog. Phys.* **77** 116503
[7] Li W H, Wang C W, Li C Y, Hsu C K, Yang C C and Wu C M 2008 *Phys. Rev. B* **77** 094508
[8] Kittel C 2004 *Introduction to Solid State Physics* (New York: John Wiley & Sons Ltd)
[9] Hong Y, Ding S, Wu W, Hu J, Voevodin A A, Gschwender L, Snyder Ed, Chow L and Su M 2010 *ACS Appl. Mater. Interface* **2** 1685
[10] Ho W J, Lee Y Y, Hu C H and Wang W L 2016 *Opt. Express* **24** 17900-9
[11] Wu F Y, Yang C C, Wu C M, Wang C W and Li W H 2007 *J. Appl. Phys.* **101** 09G111
[12] Cingarapu S, Yang Z, Sorensen C and Klabunde K 2011 *Inorg. Chem.* **50** 5000
[13] Dybkjìr G, Kruse N, Johansen A, Johnson E, Sarholt-Kristensen L and Bourdelle K K 1996 *Surface and Coatings Technology* **83** 82
[14] Li W H, Yang C C, Tsao F C, Wu S Y, Huang P J, Chung M K and Yao Y D 2005 *Phys. Rev. B* **72** 214516
[15] Wang H and Zhu H Z 2015 *Nanoscale Res. Lett.* **10** 487
[16] Xu R, Jia G Y and Liu C L 2014 *Acta Phys. Sin.* **63** 078501 (in Chinese)
[17] Yu Y, Guo M, Yuan M W, Liu W T and Hu J B 2016 *Biosensors and Bioelectronics* **77** 215
[18] Wang J X, Li J H, Qian S, Guo G Y, Wang Q J, Tang J, Shen H, Liu X Y, Zhang X L and Chu P 2016 *ACS Appl. Mater. Interfaces* **8** 11162
[19] Ziegler J F, Biersack J P and Littmark U 1985 *The Stopping and Ranges of Ions in Solids* (New York: Pergamon)
[20] Johnson E, Hjemsted K, Schmidt B, Bourdelle K K, Johansen A, Anderson H H and Sarholt-Kristensen L 1992 *Mat. Res. Soc. Symp. Proc.* **235** 485
[21] Kemerink G J and Pleiter F 1985 *Scripta Metallurgica* **19** 881
[22] Lai S L, Carlsson J R A and Allen L H 1998 *Appl. Phys. Lett.* **72** 1098
[23] Martine J M and Doherty R D 1976 *Stability of Microstructure in Metallic Systems* (London: Cambridge University Press)
[24] Ardell A J 1972 *Acta Metall.* **20** 61
[25] Zhang D L and Cantor B 1990 *Philosophical Magazine A* **62** 557
[26] Murray J L 1983 *Bulletin of Alloy Phase Diagrams* **4** 271
[27] Peterson N L and Rothman S J 1970 *Phys. Rev. B* **1** 3264
[28] Alexander W B and Slifkin L M 1970 *Phys. Rev. B* **1** 3274
[29] Anand M S, Murarka S P and Agarwala R P 1965 *J. Appl. Phys.* **36** 3860
[30] Hood G M and Schultz R J 1971 *Phys. Rev. B* **4** 2339
[31] Fradin F Y and Rowland T J 1967 *Appl. Phys. Lett.* **11** 207
[32] Lundy T S and Murdock J F 1962 *J. Appl. Phys.* **33** 1671